Supporting Information

Synthesis of an Arenide-Masked Scandium Complex Accompanied by Reductively Induced C-H Activation

Alejandra Gómez-Torres, Alejandro Metta-Magaña, and Skye Fortier*
Department of Chemistry, University of Texas at El Paso, El Paso, Texas 79968, US

Table of contents

General considerations

X-ray crystallography S3

Synthetic procedures

- Dehydration of $ScCl_3 \cdot 6H_2O$ S4
- ScCl(^{ket}guan)(NIm^{Dipp})·0.5C_7H_8 (**Sc^{Cl}**·0.5C_7H_8) S4
- [K(18-c-6)(Et_2O)][Sc{(DippN)[2-^{i}Pr-6-(*C*Me_2)C_6H_3N]C(NC*H*^{t}Bu_2)}(NIm^{Dipp})(THF)]·0.5Et_2O (**Sc^{C-H}**·Et_2O) and [(18-c-6)K(μ-η^6:η^4-$C_{10}H_8$)Sc(^{ket}guan)(NIm^{Dipp})] (**Sc^{Naph}**) S5

NMR spectra

Figure S1. ^{1}H-NMR spectrum of **Sc^{Cl}**·0.5C_7H_8 ..... S8

Figure S2. ^{13}C-NMR spectrum of **Sc^{Cl}**·0.5C_7H_8 ..... S9

Figure S3. COSY NMR spectrum of **Sc^{Cl}**·0.5C_7H_8 ..... S10

Figure S4. HSQC NMR spectrum of **Sc^{Cl}**·0.5C_7H_8 ..... S11

Figure S5. ^{1}H-NMR spectrum of **Sc^{C-H}·Et$_2$O** (**Sc^{C-H}-taut**) (C_6D_6) S12

Figure S6. ^{13}C DEPT-135 NMR spectrum of **Sc^{C-H}·Et$_2$O** (**Sc^{C-H}-taut**) S13

Figure S7. COSY NMR spectrum of **Sc^{C-H}·Et$_2$O** (**Sc^{C-H}-taut**) S14

Figure S8. TOCSY NMR spectrum of **Sc^{C-H}·Et$_2$O** (**Sc^{C-H}-taut**) S15

Figure S9. ^{1}H-NMR spectrum of **Sc^{C-H}·Et$_2$O** (**Sc^{C-H}-taut**) (THF-d_8) S16

Figure S10. Variable temperature spectral array of **Sc^{C-H}·Et$_2$O** (**Sc^{C-H}-taut**) S17

Figure S11. ^{1}H-NMR spectrum of **Sc^{naph}** S18

Figure S12. ^{13}C-NMR spectrum of **Sc^{naph}** S19

Figure S13. COSY NMR spectrum of **Sc^{naph}** S20

Figure S14. HSQC NMR spectrum of **Sc^{naph}** S21

Figure S15. Spectral array following the room temperature decomposition of **Sc^{naph}** to form **Sc^{C-H}·THF** and naphthalene S22

Crystallographic data

Figure S16. Solid-state molecular structure of **Sc^{Cl}**·0.5C_7H_8 ..... S23

Figure S17. Solid-state molecular structure of **Sc^{C-H}·THF** S24

Figure S18. Solid-state molecular structure of **Sc^{C-H}·Et$_2$O** S25

Figure S19. Solid-state molecular structure of **Sc^{naph}** S26

Figure S20. Solid-state molecular structure of [(^{ket}guan)(^{Dipp}ImN)Sc(μ-Cl)$_2$K(DME)]·C_6H_{14} S27

Table S1. X-ray crystallographic data for complexes **Sc^{Cl}**, **Sc^{C-H}·Et$_2$O**, **Sc^{C-H}·THF**, **Sc^{Naph}**, and [(^{ket}guan)(^{Dipp}ImN)Sc(μ-Cl)$_2$K(DME)]·C_6H_{14} S28

UV/vis/NIR spectroscopy

Figure S21. Room temperature electronic absorption spectrum of **Sc^{Cl}**·0.5C_7H_8 ..... S30

Figure S22. Room temperature electronic absorption spectrum of **Sc^{C-H}·Et$_2$O** (**Sc^{C-H}-taut**) S31

Figure S23. Room temperature electronic absorption spectrum of **Sc^{naph}** S32

References S33

General considerations

All air- and moisture-sensitive operations were carried out in a MBraun glovebox under an atmosphere of ultra-high purity nitrogen. Toluene, hexanes, *n*-pentane, tetrahydrofuran (THF), diethyl ether (Et_2O), and dimethoxyethane (DME) solvents were dried using a Pure Process Technology Solvent Purification System. Dioxane was distilled over sodium benzophenone ketyl. All solvents were subsequently stored under a dinitrogen atmosphere over activated 4 Å molecular sieves for at least 24 h prior to use. The deuterated solvents, C_6D_6 and THF-d_8, were purchased from Cambridge Isotope Laboratories Inc., degassed via three freeze-pump-thaw cycles, and dried over activated 4 Å molecular sieves for over 24 h prior to use. Celite and 4 Å molecular sieves were heated under dynamic vacuum to 150 ºC for over 72 h and then cooled under vacuum. Complexes $ScCl_2(NIm^{Dipp})(THF)_3$[1] and $Li(THF)_2(^{ket}guan)$[2] were synthesized following reported procedures. 18-crown-6 was purchased from Oakwood Products, Inc. and made anhydrous using the Gokel method.[3] All other reagents were purchased from commercial sources and used as provided. NMR spectra were recorded on Bruker AVANCE III 400 MHz spectrometer. ^1H and $^{13}C\{^1H\}$ NMR spectra are referenced to $SiMe_4$ using the residual ^1H solvent peaks as internal standards or the characteristic ^{13}C signals of the solvent. In addition, resonance assignments in the $^{13}C\{^1H\}$ NMR spectra are based upon ^1H-^{13}C HSQC 2D correlation spectra for **Sc^{Cl}**·$0.5C_7H_8$ and **Sc^{naph}**, while the $^{13}C\{^1H\}$ NMR signals for **Sc$^{C\text{-}H}$·Et$_2$O** are based upon the ^{13}C DEPT-45, ^{13}C DEPT-90, and ^{13}C DEPT-135 polarization transfer methods. UV-vis spectra were recorded with a Cary 5000 UV-vis-NIR spectrophotometer in toluene or THF. Elemental analyses were performed by Midwest Microlabs, LLC.

X-ray crystallography

Data for **Sc^{Cl}**·$0.5C_7H_8$, **Sc$^{C\text{-}H}$·Et$_2$O**, **Sc$^{C\text{-}H}$·THF**, **Sc^{naph}** and [(^{ket}guan)(^{Dipp}ImN)Sc(μ-Cl)$_2$K(DME)]·C_6H_{14} were collected on a dual source Bruker D8 Venture 4-axis diffractometer equipped with a PHOTON II CPAD detector and a lμS Mo Kα X-ray source (α = 0.71073 Å) fitted with a HELIOS MX monochromator. Crystals were mounted on a Mitigen Kapton loop, coated in NVH oil, and maintained at 100(2) K under a flow of nitrogen gas during data collection. Data collection and cell parameter determination were conducted using the SMART[4] program. Integration of the data and final cell parameter refinements were performed using SAINT[5] software with data absorption correction implemented through SADABS.[6] Structures were solved using intrinsic phasing methods and difference Fourier techniques. All hydrogen atom positions were idealized and rode on the atom of attachment. Structure solution, refinement, graphics, and creation of publication materials were performed using SHELXTL[7] or the Olex[8] crystallographic package. Relevant crystallographic data obtained for **Sc^{Cl}**, **Sc$^{C\text{-}H}$·Et$_2$O**, **Sc$^{C\text{-}H}$·THF**, **Sc^{Naph}**, and [(^{ket}guan)(^{Dipp}ImN)Sc(μ-Cl)$_2$K(DME)]·C_6H_{14} is presented in Table S1, and complete crystallographic data for complexes **Sc^{Cl}**·$0.5C_7H_8$, and **Sc$^{C\text{-}H}$·Et$_2$O** has been deposited in the Cambridge Crystallographic Data Center under the following CCDC deposit numbers: 2176216 (**Sc^{Cl}**·$0.5C_7H_8$), 2176217 (**Sc$^{C\text{-}H}$·Et$_2$O**), 2194112 (**Sc$^{C\text{-}H}$·THF**), 2194113 (**Sc^{naph}**), 2194416 ([(^{ket}guan)(^{Dipp}ImN)Sc(μ-Cl)$_2$K(DME)]·C_6H_{14}).

In **Sc^{Cl}**·$0.5C_7H_8$, positional disorder of the ketimine *tert*-butyl substituents was addressed by modeling carbon atoms C43, C44, C48, and C49 over two orientations with occupancies determined through data refinement. In addition, the non-coordinating half toluene molecule was found to exhibit positional disorder and was modeled over four positions with 0.25 occupancies and SADI (0.02) restraints applied to four unique carbon atoms within the ring (C62A, C64A, C65A, and C66A). For complex **Sc$^{C\text{-}H}$·Et$_2$O**, positional disorder was found in the K2-coordinated 18-crown-6 fragment (O10-O15, C139-C150), the Sc2-coordinated THF molecule (C159-C162),

and both the K1-, and K2-coordinated Et_2O molecules (O8, C75-C77, C153, C154), as well as two isopropyl substituents (C89, C90, C94-C98, C104), all of which were modeled over two orientations with occupancies determined through data refinement. In compound [(^{ket}guan)(^{Dipp}ImN)Sc(μ-Cl)$_2$K(DME)]·C_6H_{14}, reflections 4 0 8, and 0 6 0 were omitted as outliers. Moreover, atoms C47-C49 belonging to the ketimine-guanidinate ligand were modeled by splitting the electron density over two orientations with occupancies determined through data refinement. Similarly, positional disorder exhibited by the Sc1-coordinated THF molecule (O1, C62-C65), and one isopropyl substituent (C19, C20) in **Sc$^{C\text{-}H}$·THF** as well as the *tert*-butyl (C69-C71) substituent, isopropyl atom C37, and 18-crown-6 fragment (O1-O6, C72-C83) in **Sc^{naph}** was modeled over two orientations with occupancies determined through data refinement. Residual electron density corresponding to highly disordered THF/pentanes in compounds **Sc$^{C\text{-}H}$·THF** and **Sc^{naph}** could not be accurately modeled and instead the density was removed using the PLATON/SQUEEZE algorithm.[9] The solid-state molecular structures of complexes **Sc$^{C\text{-}H}$·THF** and **Sc^{naph}** is presented here for connectivity purposes only.

Synthetic procedures

Dehydration of $ScCl_3·6H_2O$

A 100 mL Schlenk flask containing a medium magnetic stir bar was loaded with Me_3SiCl (7.34 mL, 6.28 g, 57.83 mmol), dioxane (15 mL), and $ScCl_3·6H_2O$ (1.00 g, 3.85 mmol) under a positive nitrogen pressure. The heterogeneous reaction mixture was refluxed under dinitrogen for 2 d. After this time, the suspension was dried under reduced pressure yielding a white powder identified as $ScCl_3·1H_2O·3THF$. THF (15 mL) and Me_3SiCl (2.45 mL, 2.09 g, 22.49 mmol) were added to dried $ScCl_3·1H_2O·3THF$ under positive nitrogen pressure. The heterogeneous mixture was refluxed under dinitrogen for 16 h. The resulting suspension was dried under reduced pressure, suspended in fresh THF (10 mL), stirred at room temperature for 10 minutes, and filtered through a medium porosity glass frit affording $ScCl_3(THF)_3$ as a white powder. Yield: 1.22 g, 86.1%.

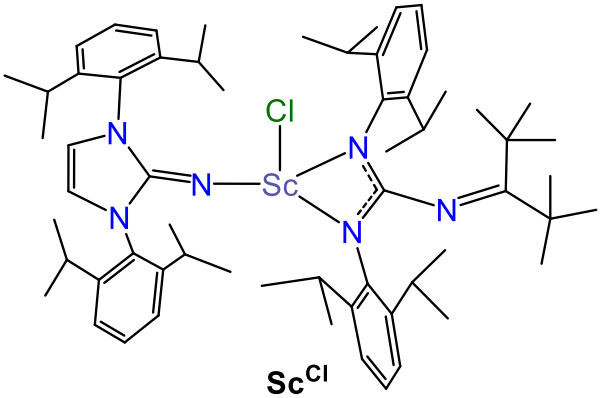

Sc^{Cl}

Synthesis of ScCl(^{ket}guan)(NIm^{Dipp})·0.5C_7H_8 (Sc^{Cl}·0.5C_7H_8)

A 50 mL Cajon flask containing a small magnetic stir bar was loaded with (Im^{Dipp}N)Sc(Cl_2)$(THF)_3$ (1.00 g, 1.24 mmol), (^{DippKet}guan)Li$(THF)_2$ (0.81g, 1.24 mmol), and C_7H_8 (25 mL). The homogeneous light-yellow solution was stirred at 60 °C for 16 h, after which time the resulting suspension was allowed to cool down to room temperature. The resulting mixture was filtered through Celite supported on a medium porosity glass frit. The solvent was removed under reduced pressure affording a pale-yellow material that was redissolved in pentane (8-10 mL) and stored at -35 °C for 12 h to produce a crop of colorless crystals of **Sc^{Cl}**·0.5C_7H_8. Yield:

1.18 g, 88.4%. Note: compound **Sc^{Cl}**·0.5C_7H_8 is highly soluble in ethereal (THF and Et_2O), aromatic (C_7H_8 and C_6H_6), and non-polar solvents (hexanes and pentanes).

^{1}H NMR (25 °C, 400 MHz, C_6D_6): δ 0.70 (s, 9H, C*Me*$_3$), 0.76 (s, 9H, C*Me*$_3$), 1.12 – 1.15 (m, 18H, two overlapping *Me*$_2$CH), 1.20 (d, 6H, *Me*$_2$CH, J_{HH} = 6.2 Hz), 1.34 – 1.37 (m, 18H, two overlapping *Me*$_2$CH), 1.41 (d, 6H, *Me*$_2$CH, J_{HH} = 6.3 Hz), 3.23 (sept, 4H, Me$_2$C*H*, J_{HH} = 6.8 Hz), 3.72 (sept, 2H, Me$_2$C*H*, J_{HH} = 6.7 Hz), 4.01 (sept, 2H, Me$_2$C*H*, J_{HH} = 6.7 Hz), 5.77 (s, 2H, Imid *HC*=C*H*), 7.06 – 7.10 (m, 8H, overlapping *aryl* signals), 7.18 (t, 4H, *aryl*). **^{13}C{^{1}H} NMR (25 °C, 101 MHz, C_6D_6):** δ 21.82 (*Me*$_2$CH), 22.04 (Me$_2$*C*H), 23.91 (*Me*$_2$CH), 24.74 (*Me*$_2$CH), 25.94 (*Me*$_2$CH), 28.51 (Me$_2$*C*H), 28.64 (Me$_2$*C*H), 28.83 (Me$_2$*C*H), 28.87 (C*Me*$_3$), 29.32 (Me$_2$*C*H), 30.59 (C*Me*$_3$), 43.49 (*C*Me$_3$), 43.87 (*C*Me$_3$), 114.03 (Imid H*C*=*C*H), 122.40 (*aryl*), 123.47 (*aryl*), 124.36 (*aryl*), 125.04 (*aryl*), 135.33 (*aryl*), 141.52 (*aryl*), 143.42 (*aryl*), 144.41 (*C*N$_3$), 147.43 (*aryl*), 164.33 (^{t}Bu$_2$*C*=N), 181.60 (*C*N$_3$). **UV-vis (C_7H_8, 0.207 mM, 25 °C, nm, ε = L·mol^{-1}·cm^{-1}):** 295 (ε = 17,778). **Anal. Calcd. for $C_{61}ClH_{88}N_6Sc$·0.5C_7H_8:** C, 75.13; H, 9.04; N, 8.09. Found: C, 71.87; H, 9.22; N, 8.06. Repeated combustion analyses consistently tested low in carbon content which may be a consequence of poor combustion properties.

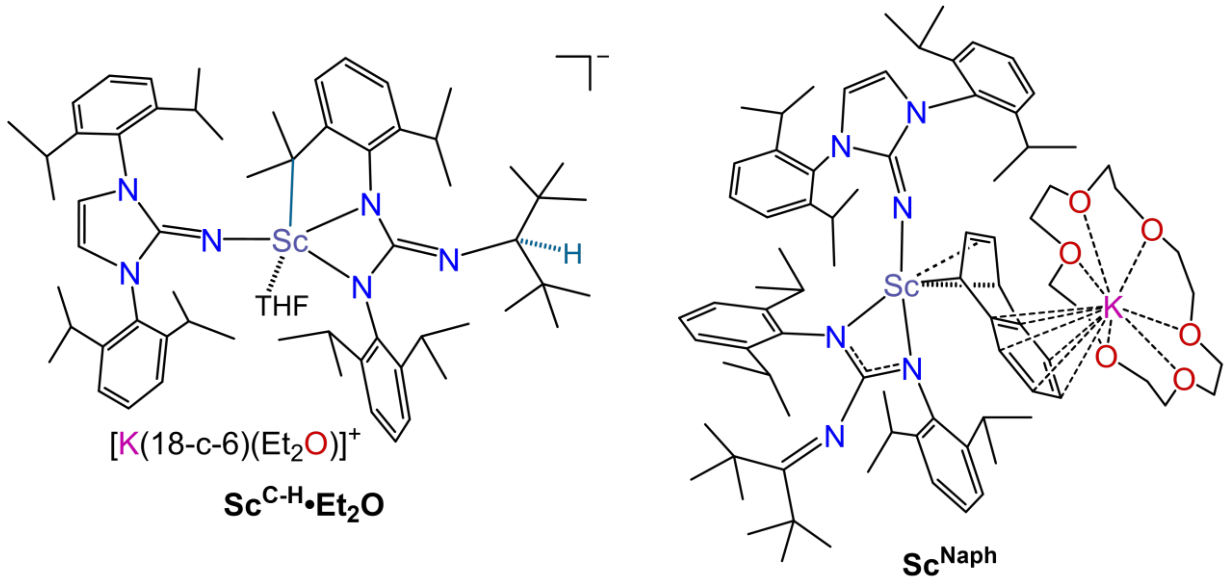

Synthesis of [K(18-c-6)(Et$_2$O)][Sc{(DippN)[2-^{i}Pr-6-(*C*Me$_2$)C$_6$H$_3$N]C(NC*H*^{t}Bu$_2$)}(NIm^{Dipp})(THF)]·0.5Et$_2$O (Sc^{C-H}·Et$_2$O) and [(18-c-6)K(μ-η^6:η^4-C$_{10}$H$_8$)Sc(^{ket}guan)(NIm^{Dipp})] (Sc^{Naph})

In a 20 mL scintillation vial, potassium metal (0.28 g, 0.73 mmol) was suspended in THF (8 mL) to which naphthalene (0.09 mg, 0.73 mmol) was added. The reaction mixture was stirred at room temperature until the metal was completely consumed. The resulting dark forest green solution was cooled to -35 °C prior to addition of **1**·0.5C_7H_8 (0.30 g, 0.29 mmol), which subsequently resulted in an immediate color change to dark red. The homogeneous solution was stirred at -35 °C for 16 h, time after which 18-crown-6 (0.768 g, 0.29 mmol) was added. The reaction mixture was then concentrated to 4 mL under vacuum and layered with pentanes (3 mL). A mixture of colorless plates of **Sc^{C-H}**·2THF·C_5H_{12} (**Sc^{C-H}·THF**) and dark red rhombohedral crystals of **Sc^{naph}** were obtained upon overnight storage at -35 °C. Colorless crystals of **Sc^{C-H}·THF** grow rapidly from saturated solutions of THF/pentane (1:1), usually depositing crystals within an hour that are accompanied by small amounts of red **Sc^{naph}**. Repeated fractional crystallization of **Sc^{C-H}** in this fashion removes **Sc^{naph}**, that when obtained in reasonable purity, can be finally recrystallized from a concentrated Et_2O/pentanes (1:1) mixture. This mixture, when stored several days at -35 °C, produces **Sc^{C-H}·Et$_2$O**. All attempts to isolate pure crystalline material of **Sc^{naph}**

were unsuccessful due to the persistent presence of **Sc$^{C\text{-}H}$**. Isolated yield: 115 mg (**Sc$^{C\text{-}H}$·Et$_2$O**, 27.0%), 148 mg (**Sc^{naph}**, 35.8%). Compounds **Sc$^{C\text{-}H}$** and **Sc^{naph}** are highly soluble in ethereal solvents such as THF and Et_2O, partially soluble in aromatic solvents such as C_7H_8 and C_6H_6, while insoluble in non-polar solvents like hexanes and pentanes. In all cases, **Sc^{naph}** exhibits slightly higher solubility as compared to **Sc$^{C\text{-}H}$**. In solution, **Sc$^{C\text{-}H}$·Et$_2$O** tautomerizes to [K(18-c-6)(Et_2O)][Sc{(DippN)[2-^{i}Pr-6-(CH_3CHCH_2)C_6H_3N]C(NC$H^{t}Bu_2$)}(NIm^{Dipp})(THF)] (**Sc$^{C\text{-}H}$-taut**).

Sc$^{C\text{-}H}$·Et$_2$O (Sc$^{C\text{-}H}$-taut):

^{1}H NMR (25 °C, 400 MHz, C_6D_6): δ 0.24 (m, 2H, overlapping Sc-CH_2CHCH$_3$), 0.68 (d, 3H, *Me*CHMe, J_{HH} = 6.5 Hz), 1.06 (s, 9H, CMe_3), 1.12 (t, Et_2O), 1.23 (d, 6H, Me_2CH, J_{HH} = 6.5 Hz), 1.34 – 1.38 (m, 25H, overlapping CMe_3, Me_2CH, and THF signals), 1.49 (d, 3H, *Me*CHMe, J_{HH} = 6.7 Hz), 1.57 (d, 6H, Me_2CH, J_{HH} = 6.4 Hz), 1.65 (d, 3H, *Me*CHMe, J_{HH} = 6.6 Hz), 1.71 (m, 6H, overlapping *Me*CHMe and Sc-CH$_2$CHCH_3), 1.79 (d, 3H, *Me*CHMe, J_{HH} = 6.1 Hz), 1.87 (d, 3H, *Me*CHMe, J_{HH} = 6.7 Hz), 2.95 (s, 24H, 18-crown-6), 3.25 (q, Et_2O), 3.44 (s, 1H, $^{t}Bu_2CH$), 3.56 (br m, 2H, Me_2CH overlapping with THF signal), 3.60 (m, 4H, THF overlapping with Me_2CH signal), 3.78 (sept, 2H, Me_2CH, J_{HH} = 6.3 Hz), 3.93 (sept, 1H, Me_2CH, J_{HH} = 6.7 Hz), 4.50 (br s, 1H, Sc-CH$_2$CHCH$_3$), 4.83 (sept, 1H, Me_2CH, J_{HH} = 6.7 Hz), 5.08 (sept, 1H, Me_2CH, J_{HH} = 6.3 Hz), 6.03 (s, 2H, Imid *H*C=C*H*), 7.04 (t, 1H, *aryl*, J_{HH} = 7.4 Hz), 7.11 (t, 1H, *aryl*, J_{HH} = 7.3 Hz), 7.22 - 7.34 (9H, overlapping *aryl* signals), 7.40 (d, 1H, *aryl*, J_{HH} = 7.3 Hz). **^{1}H NMR (25 °C, 400 MHz, THF-d_8):** δ -0.60 (d, 1H, Sc-CH_2CHCH$_3$, J_{HH} = 11.5 Hz), -0.50 (t, 1H, Sc-CH_2CHCH$_3$, J_{HH} = 12.2 Hz), -0.09 (d, 3H, Sc-CH$_2$CHCH_3, J_{HH} = 6.6 Hz), 0.38 (s, 9H, CMe_3), 0.69 – 0.71 (m, 12 H, overlapping CMe_3 and Me_2CH), 0.81 (d, 3H, *Me*CHMe, J_{HH} = 6.7 Hz), 0.94 (d, 3H, *Me*CHMe, J_{HH} = 6.3 Hz), 0.98 – 1.03 (m, 9H, overlapping Me_2CH), 1.11 (m, 9H, overlapping Me_2CH) 1.17 (t, Et_2O), 1.28 (m, 12H, overlapping Me_2CH), 1.31 (d, 3H, *Me*CHMe, J_{HH} = 6.9 Hz), 1.68 (br s, coordinated THF), 2.80 (s, 1H, $^{t}Bu_2CH$), 3.20 (br sept, 2H, Me_2CH), 3.27 (sept, 1H, Me_2CH, J_{HH} = 6.8 Hz), 3.42 (br s, Et_2O) 3.44 (br s, 2H, Me_2CH), 3.56 (s, 24H, 18-crown-6), 3.79 (m, 1H, Sc-CH$_2$C*H*CH$_3$), 4.21 (sept, 1H, MeC*H*Me, J_{HH} = 6.8 Hz), 4.55 (sept, 1H, MeC*H*Me, J_{HH} = 6.7 Hz), 5.86 (s, 2H, Imid *H*C=C*H*), 6.49 (m, 2H, overlapping *aryl* signals), 6.56 (t, 2H, *aryl*, J_{HH} = 6.9 Hz), 6.66 (d, 1H, *aryl*, J_{HH} = 7.1 Hz), 6.78 (d, 1H, *aryl*, J_{HH} = 7.2 Hz), 6.95 (d, 2H, *aryl*, J_{HH} = 7.2 Hz), 7.06 (m, 4H, overlapping *aryl* signals). **^{13}C{^{1}H} NMR (25 °C, 101 MHz, C_6D_6, ppm):** δ 15.23 (Et_2O), 22.79 (isopropyl *Me*), 23.48 (isopropyl *Me*), 23.67 (isopropyl *Me*), 23.84 (isopropyl *Me*), 24.67 (isopropyl *Me*), 25.17 (THF), 25.37 (isopropyl *Me*), 25.65 (isopropyl *Me*), 25.70 (isopropyl *Me*), 26.72 (Me_2CH), 27.18 (isopropyl *Me*), 27.22 (Me_2CH), 27.88 (isopropyl *Me*), 28.26 (Me_2CH), 28.68 (Me_2CH), 31.09 (CMe_3), 31.19 (CMe_3), 38.23 (Me_2CH), 65.55 (Et_2O), 67.32 ($^{t}Bu_2CH$), 68.66 (THF), 69.56 (18-crown-6), 112.98 (Imid *H*C=C*H*), 119.18 (aryl), 120.05 (aryl), 120.85 (*aryl*), 121.06 (*aryl*), 121.36 (*aryl*), 123.06 (*aryl*), 123.42 (*aryl*), 127.57 (*aryl*), 127.98 (*aryl*), 143.93 (Sc-CH$_2$CHCH$_3$) Resonances corresponding to one isopropyl methyl along with Sc-CH_2CHCH$_3$, *C*N$_3$, *C*Me$_3$, and *ipso* and *ortho* aryl carbons were not observed. **UV-vis (C_7H_8, 0.234 mM, 25 °C, nm, ε = L·mol^{-1}·cm^{-1}):** 287 (ε = 12,142). **Anal. Calcd. for $C_{81}H_{120}KN_6O_8Sc$:** C, 69.99; H, 8.70; N, 6.05. Found: C, 65.72; H, 8.25; N, 5.91. Repeated combustion analyses consistently tested low in carbon content which may be a consequence of poor combustion properties.

Sc^{naph}:

^{1}H NMR (25 °C, 400 MHz, C_6D_6, ppm): δ 0.85 (br s, 9H, CMe_3), 1.02 (br s, 9H, CMe_3), 1.26 (m, 12H, overlapping Me_2CH), 1.51 (d, 12H, Me_2CH), 1.63 (m, 24H, overlapping Me_2CH), 3.13 (s, 24H, 18-crown-6), 3.74 (br s, 2H, Me_2CH), 3.82 (br s, 2H, Me_2CH), 4.26 (br s, 4H, Me_2CH), 5.74 (m, 2H, $C_{10}H_8$), 6.08 (m, 4H, overlapping Imid *H*C=C*H* and $C_{10}H_8$ signals), 6.99 (d, 2H, $C_{10}H_8$, J_{HH} = 7.2 Hz), 7.07-7.12 (m, 6H, overlapping *aryl*), 7.22 (m, 6H, overlapping $C_{10}H_8$ and four *aryl* signals), 7.31 (d, 2H, *aryl*). **^{13}C{^{1}H} NMR (25 °C, 101 MHz, C_6D_6, ppm):** δ 23.96 (Me_2CH), 25.66 (Me_2CH), 26.24 (Me_2CH), 26.52 (Me_2CH), 26.71 (Me_2CH), 28.45 (Me_2CH), 29.19 (CMe_3), 29.45

(*Me*$_2$CH), 30.14 (*Me*$_2$CH), 31.34 (C*Me*$_3$), 43.00 (*C*Me$_3$), 44.92 (*C*Me$_3$), 70.11 (18-crown-6), 75.36 (Me$_2$*C*H), 112.01 (*C*$_{10}$H$_8$), 114.34 (Imid H*C*=*C*H), 118.85 (*C*$_{10}$H$_8$), 122.36 (*C*$_{10}$H$_8$), 122.91 (*aryl*), 123.84 (*aryl*), 124.09 (*C*$_{10}$H$_8$), 124.18 (*aryl*), 127.32 (*aryl*), 134.77 (aryl), 139.37 (aryl), 144.63 (aryl), 146.43 (aryl), 146.81 (aryl), 148.44 (aryl), 150.68 (CN_3), 165.93 (^{t}Bu$_2$CN), 174.21 (CN_3). UV-vis (C_7H_8, 25 °C, nm): 284, 480.

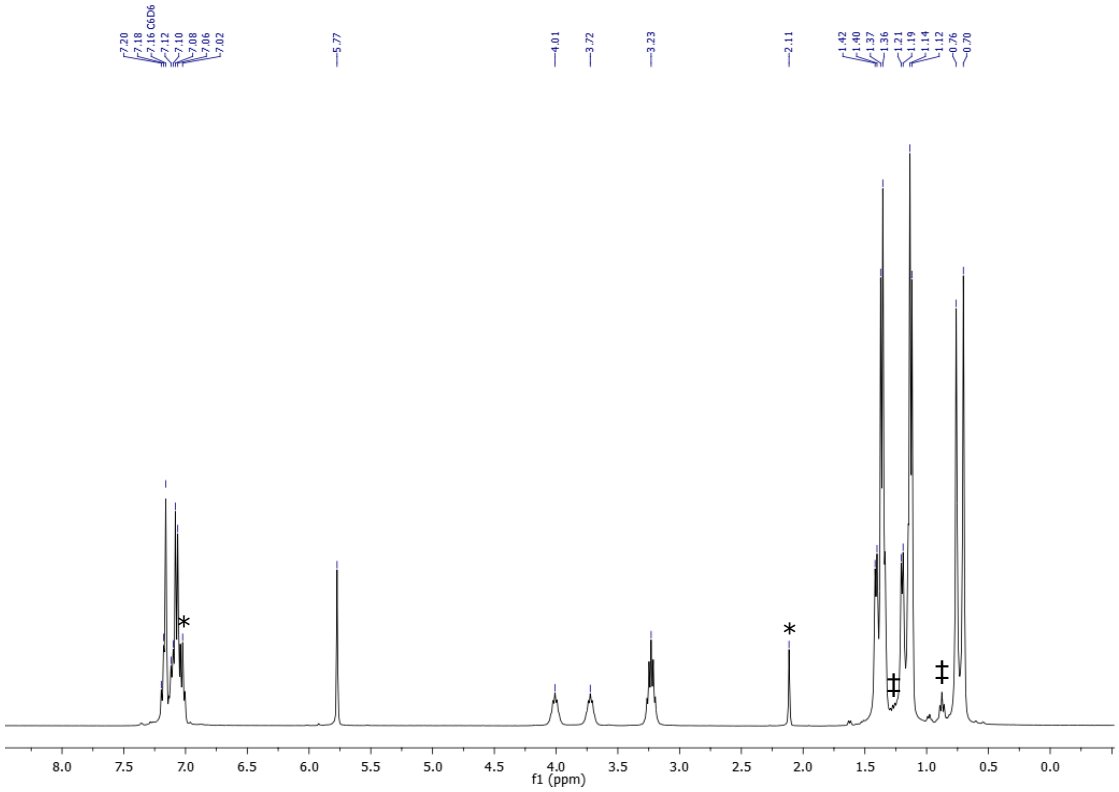

Figure S1. ^{1}H-NMR spectrum of **Sc^{Cl}**·0.5C_7H_8 (25 ˚C, 400 MHz, C_6D_6). ∗, and ‡ denote the presence of co-crystallized toluene and residual pentanes, respectively.

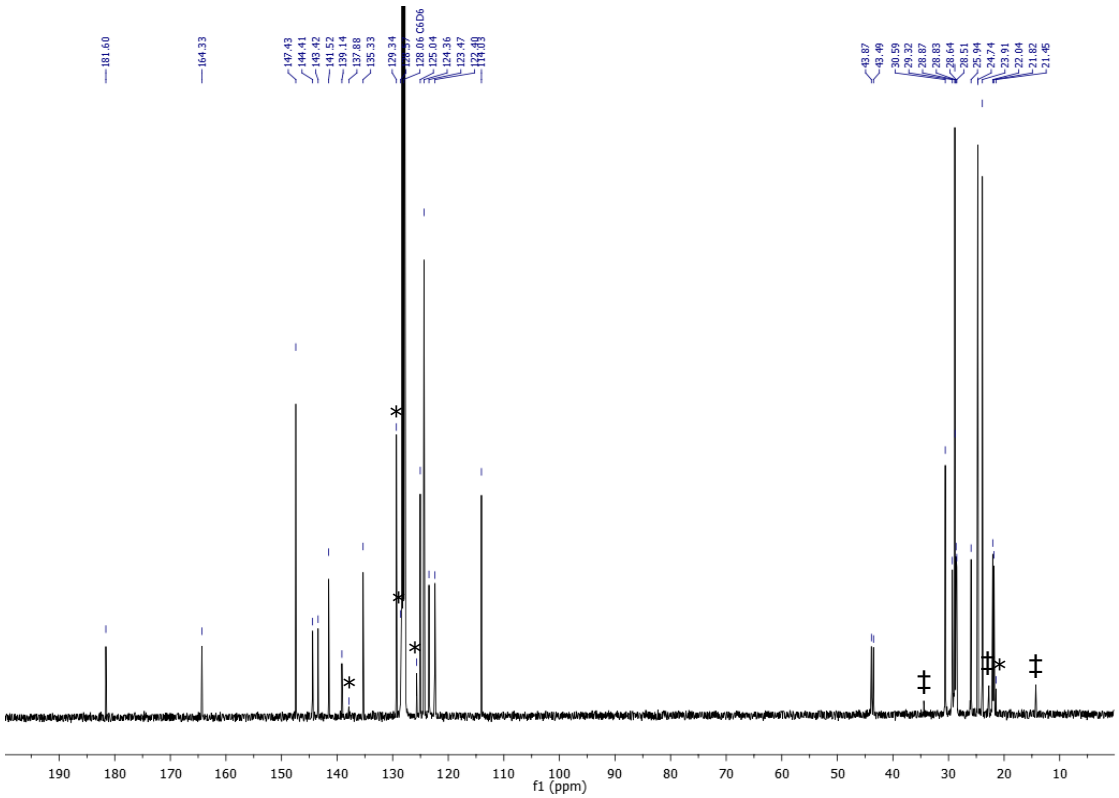

Figure S2. $^{13}C\{^{1}H\}$-NMR spectrum of **Sc^{Cl}**·0.5C_7H_8 (25 ˚C, 101 MHz, C_6D_6). ∗ and ‡ denote the presence of co-crystallized toluene and residual pentane, respectively.

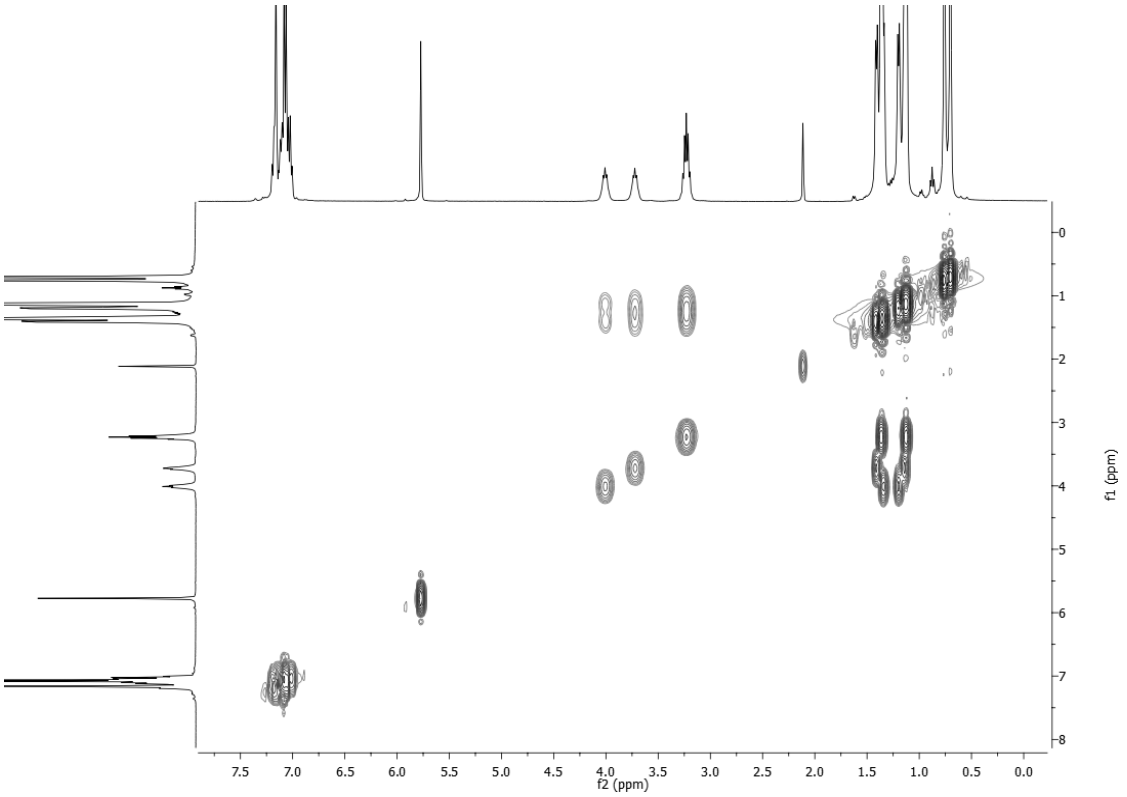

Figure S3. COSY NMR spectrum of $\mathbf{Sc^{Cl}}\cdot 0.5C_7H_8$ (25 ˚C, C_6D_6).

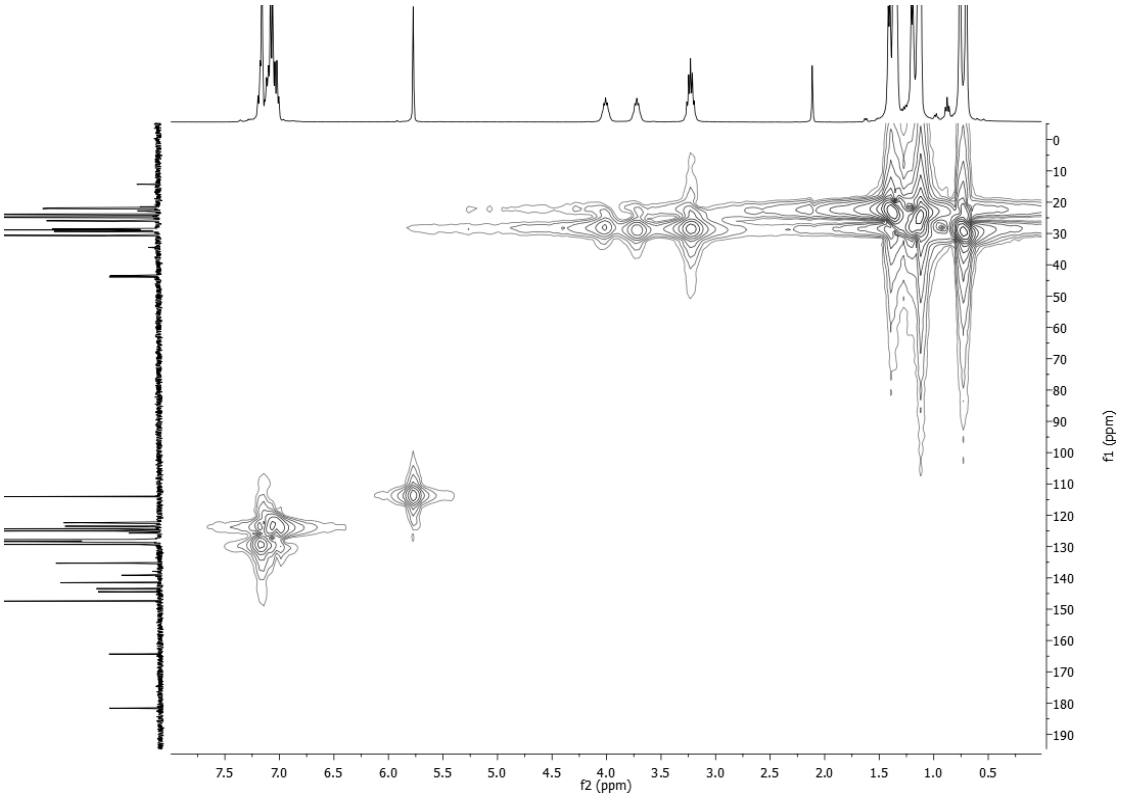

Figure S4. HSQC NMR spectrum of $\mathbf{Sc^{Cl}}\cdot 0.5C_7H_8$ (25 ˚C, C_6D_6).

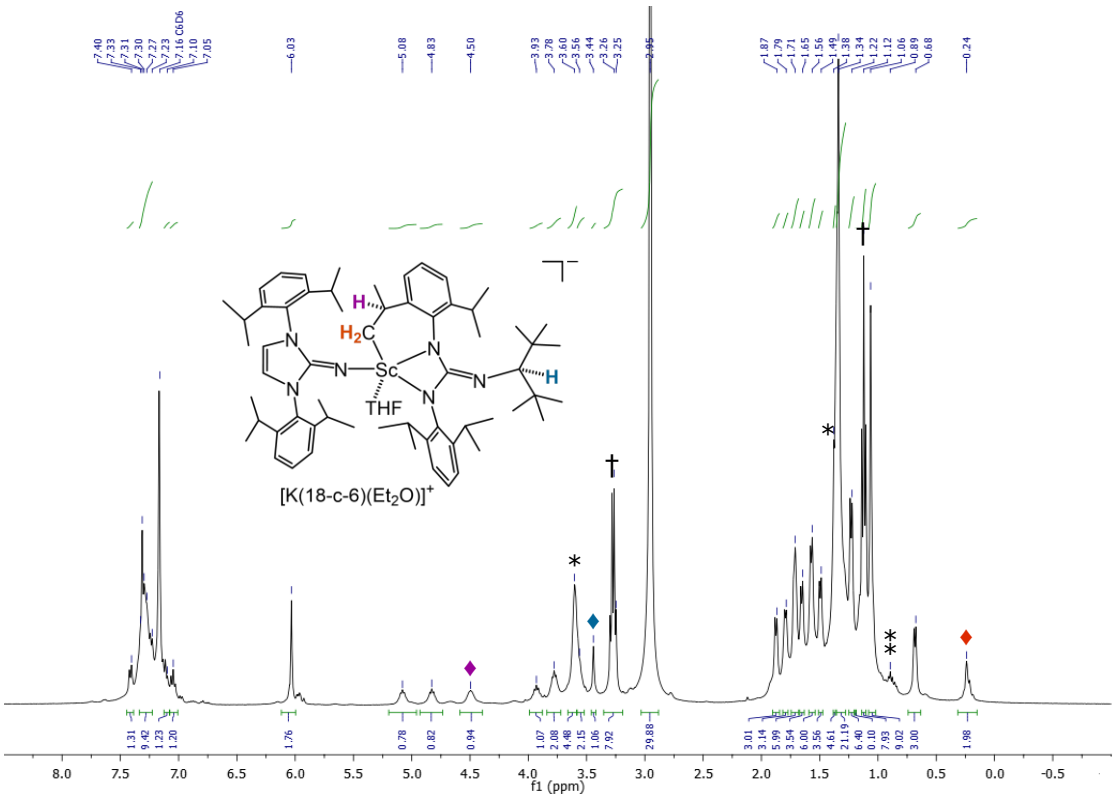

Figure S5. ^{1}H-NMR spectrum of **Sc$^{C\text{-}H}$·Et$_2$O** (**Sc$^{C\text{-}H}$-taut**) (25 ˚C, 400 MHz, C_6D_6). ∗, † denote the presence of coordinated THF and Et_2O, while ⁑ denotes the presence of residual hexanes. ♦ and ♦ diamonds correspond to the respective color-labeled protons shown in the line drawing.

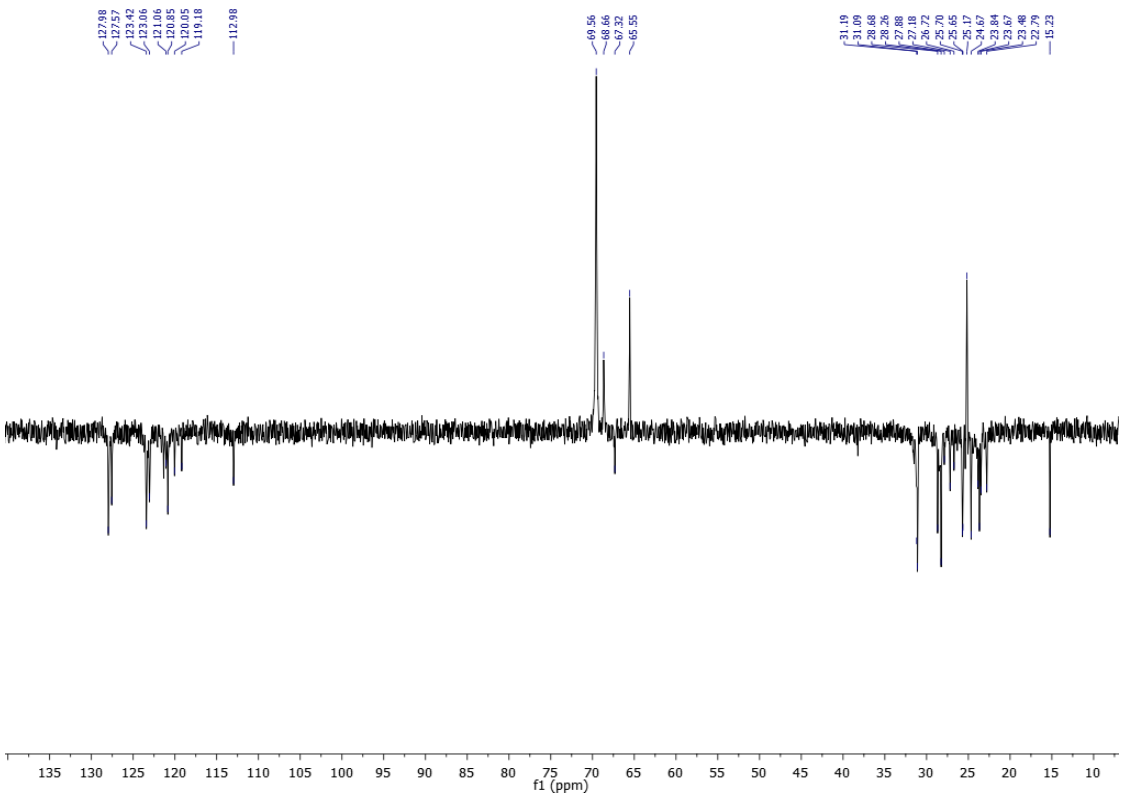

Figure S6. ^{13}C DEPT-135 NMR spectrum of **Sc$^{C\text{-}H}$·Et$_2$O** (**Sc$^{C\text{-}H}$-taut**) (25 ˚C, 101 MHz, C_6D_6).

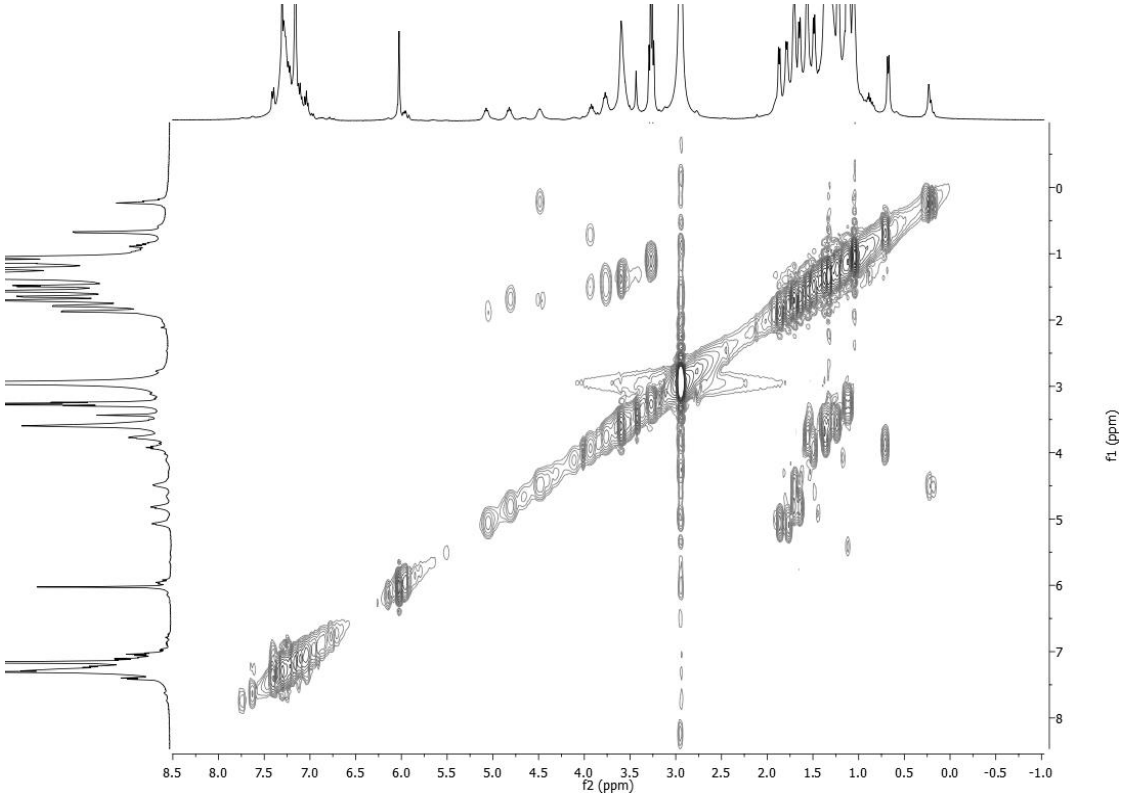

Figure S7. COSY NMR spectrum of **$Sc^{C\text{-}H}$·Et_2O** (**$Sc^{C\text{-}H}$-taut**) (25 ˚C, C_6D_6).

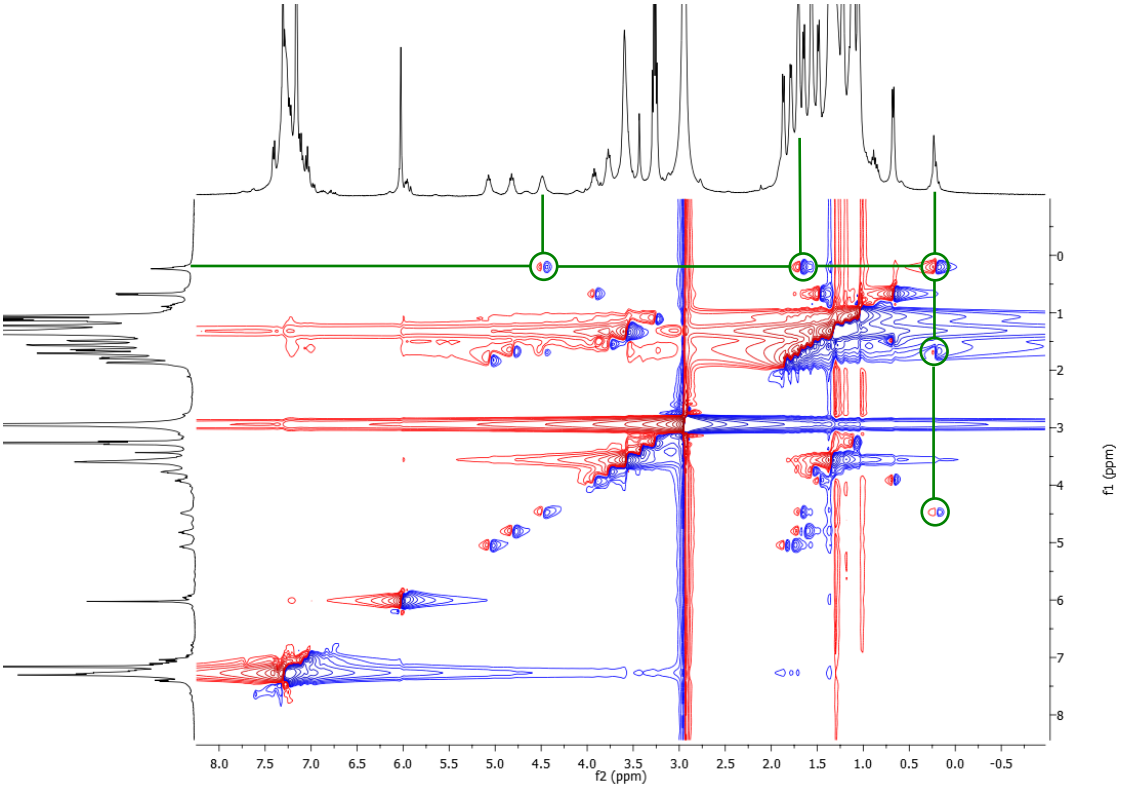

Figure S8. TOCSY NMR spectrum of **$Sc^{C\text{-}H}$·Et_2O** (**$Sc^{C\text{-}H}$-taut**) (25 ˚C, C_6D_6).

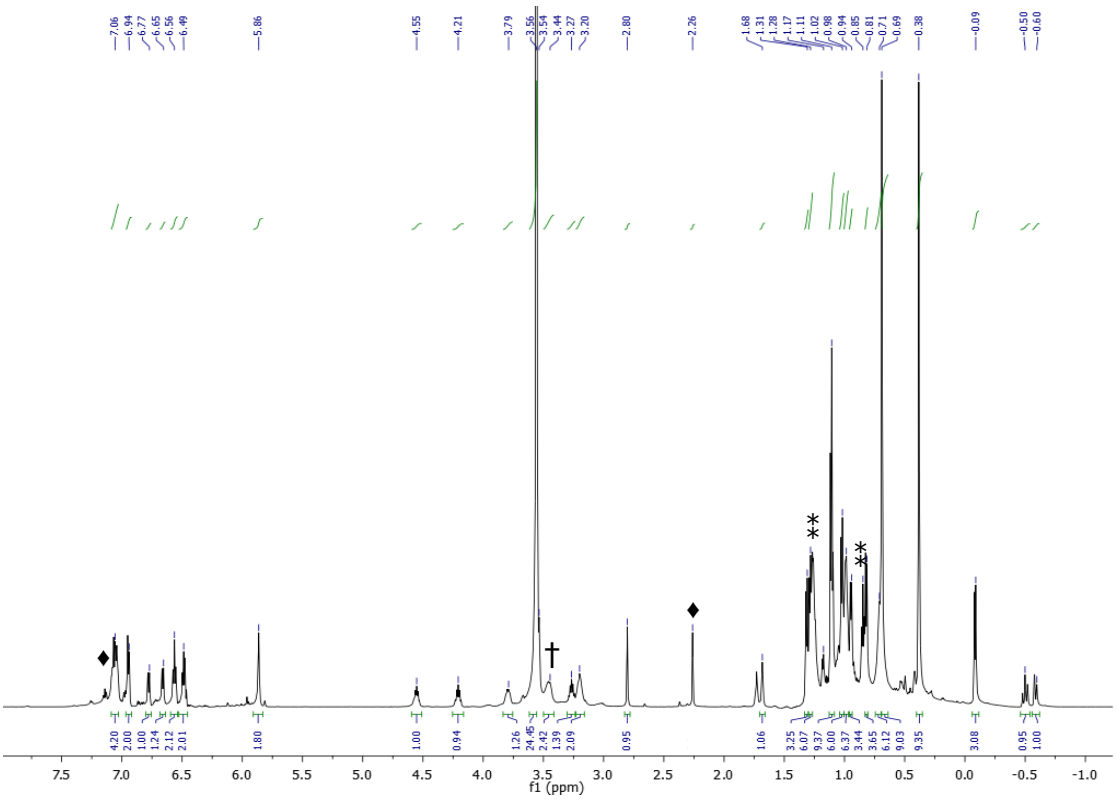

Figure S9. ^{1}H-NMR spectrum of **Sc$^{C\text{-}H}$·Et$_2$O** (**Sc$^{C\text{-}H}$-taut**) (400 MHz, THF-d_8). † denote the presence of coordinated Et_2O, while ⁑, and ♦ denote the presence of residual hexanes and toluene.

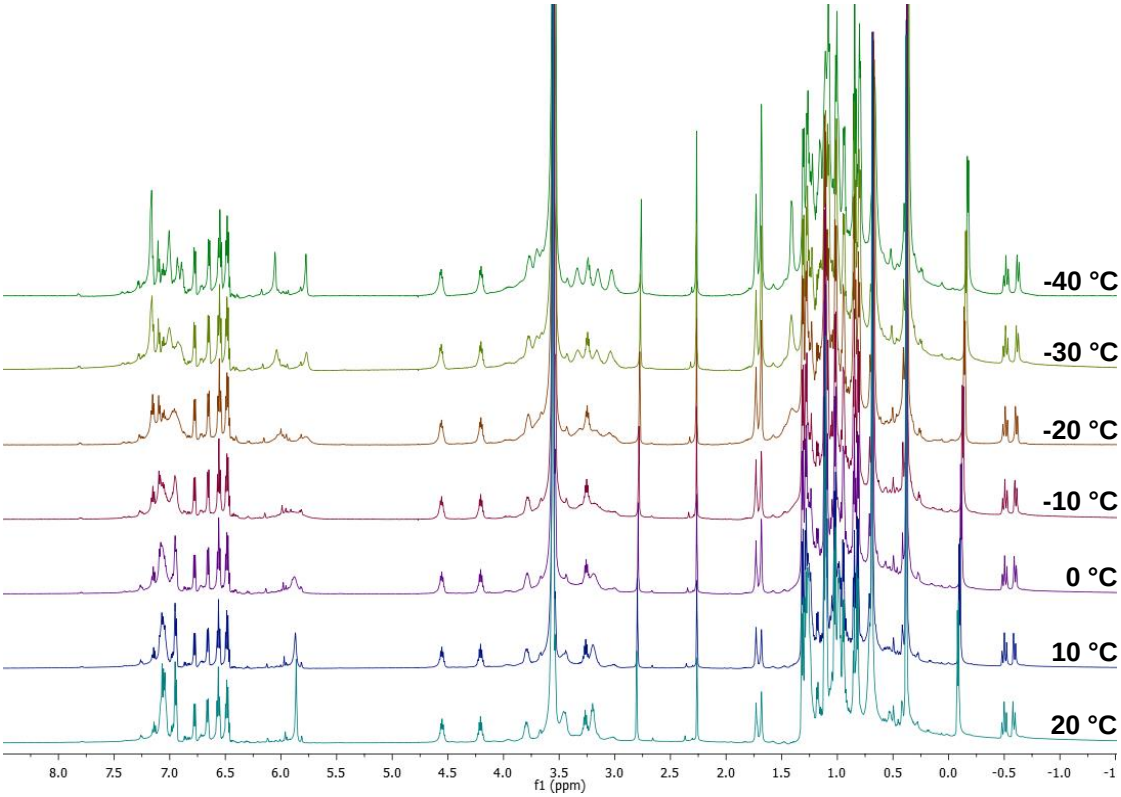

Figure S10. Variable temperature spectral array of **Sc$^{C\text{-}H}$·Et$_2$O** (**Sc$^{C\text{-}H}$-taut**) (400 MHz, THF-d_8).

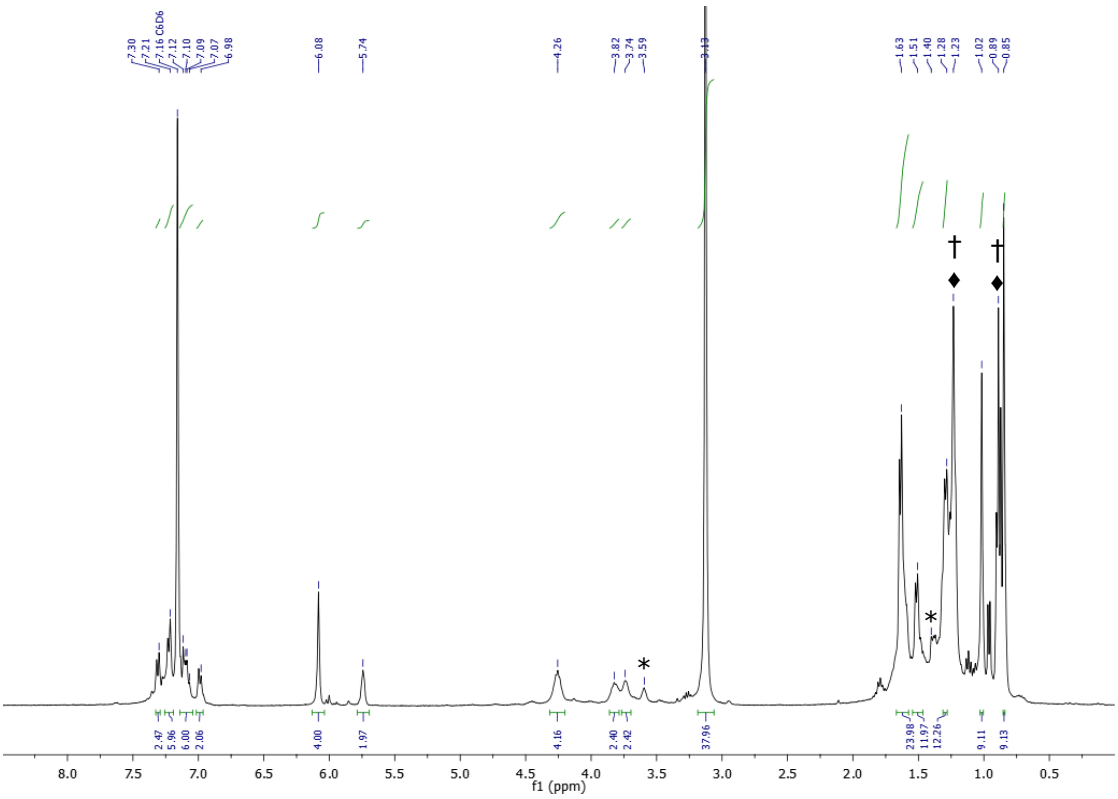

Figure S11. ^{1}H-NMR spectrum of **Sc^{naph}** (25 ˚C, 400 MHz, C_6D_6). ∗, and † denote the presence of co-crystallized THF and pentane, while ♦ denotes the presence of residual hexane.

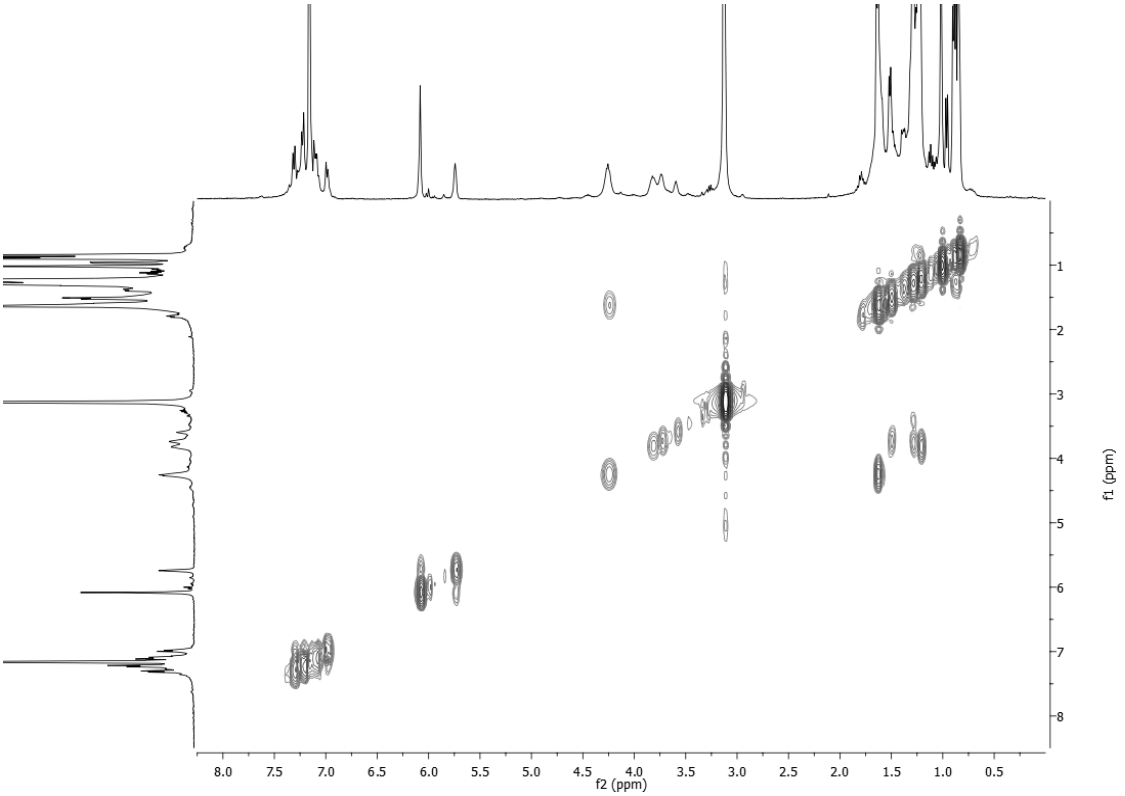

Figure S12. COSY NMR spectrum of **Sc^{naph}** (25 ˚C, C_6D_6).

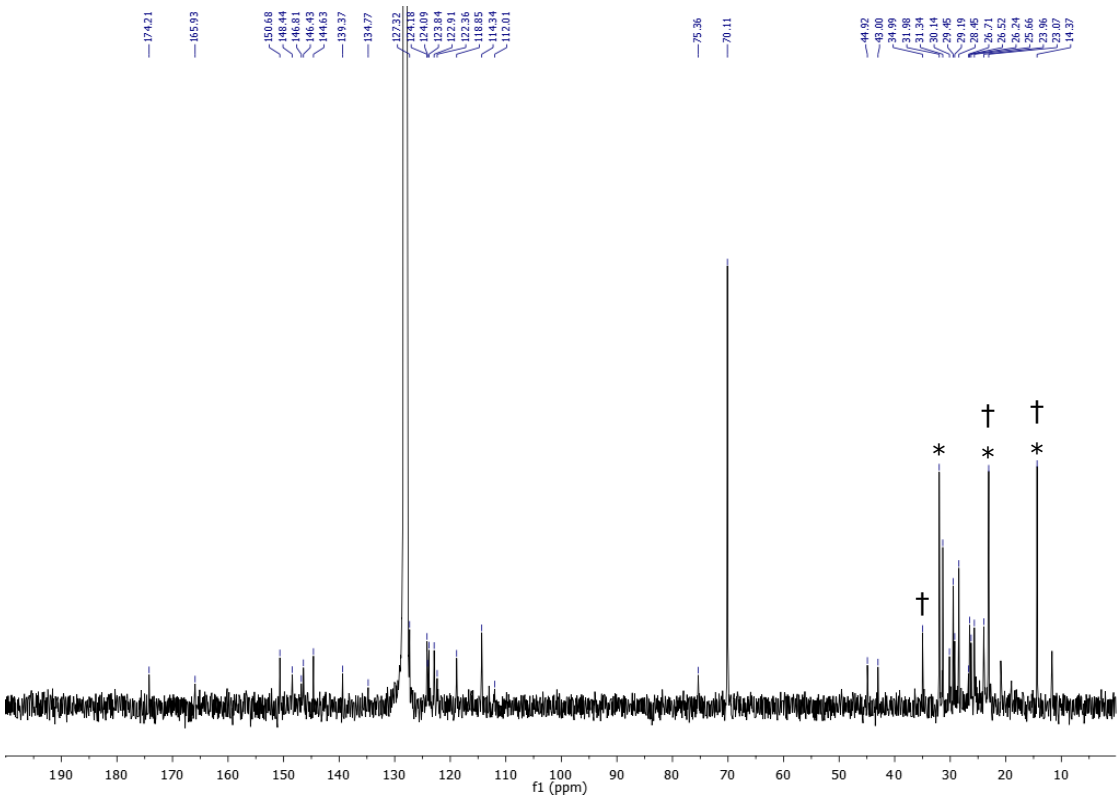

Figure S13. $^{13}C\{^{1}H\}$-NMR spectrum of **Sc^{naph}** (25 ˚C, 101 MHz, C_6D_6). †, and ∗, denote the presence of co-crystallized pentane and residual hexane, respectively.

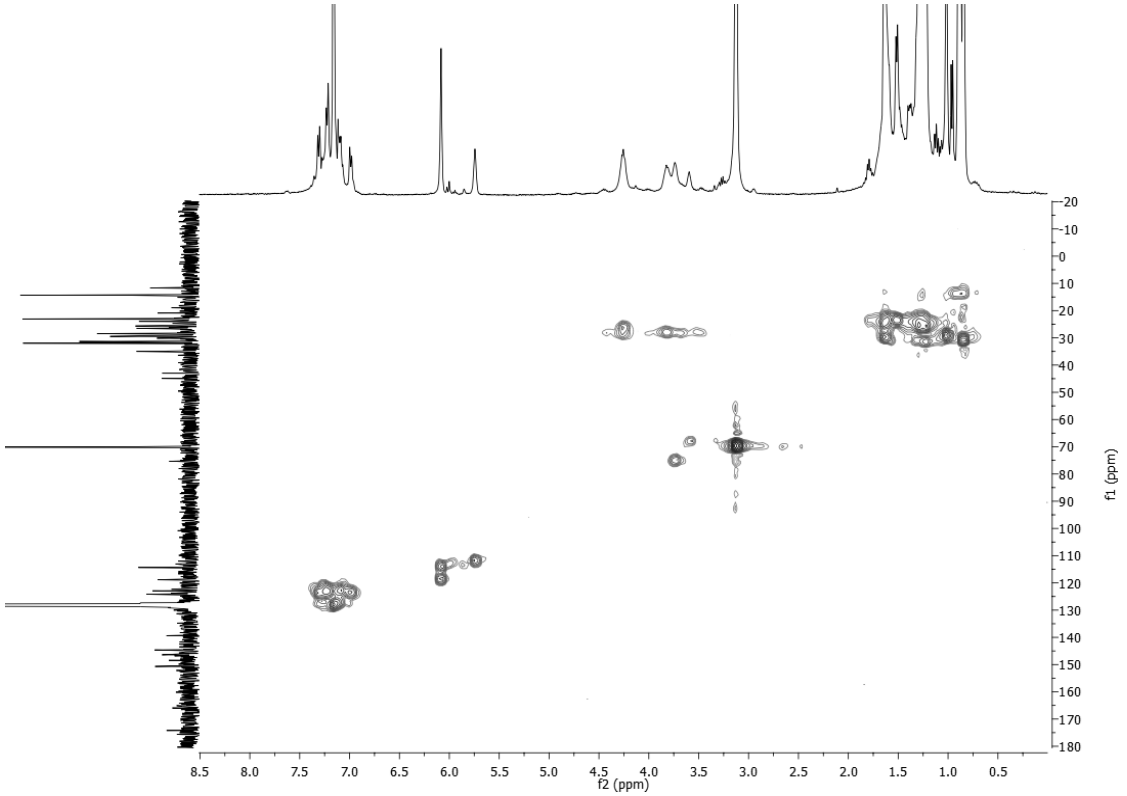

Figure S14. HSQC NMR spectrum of **Sc^{naph}** (25 ˚C, C_6D_6).

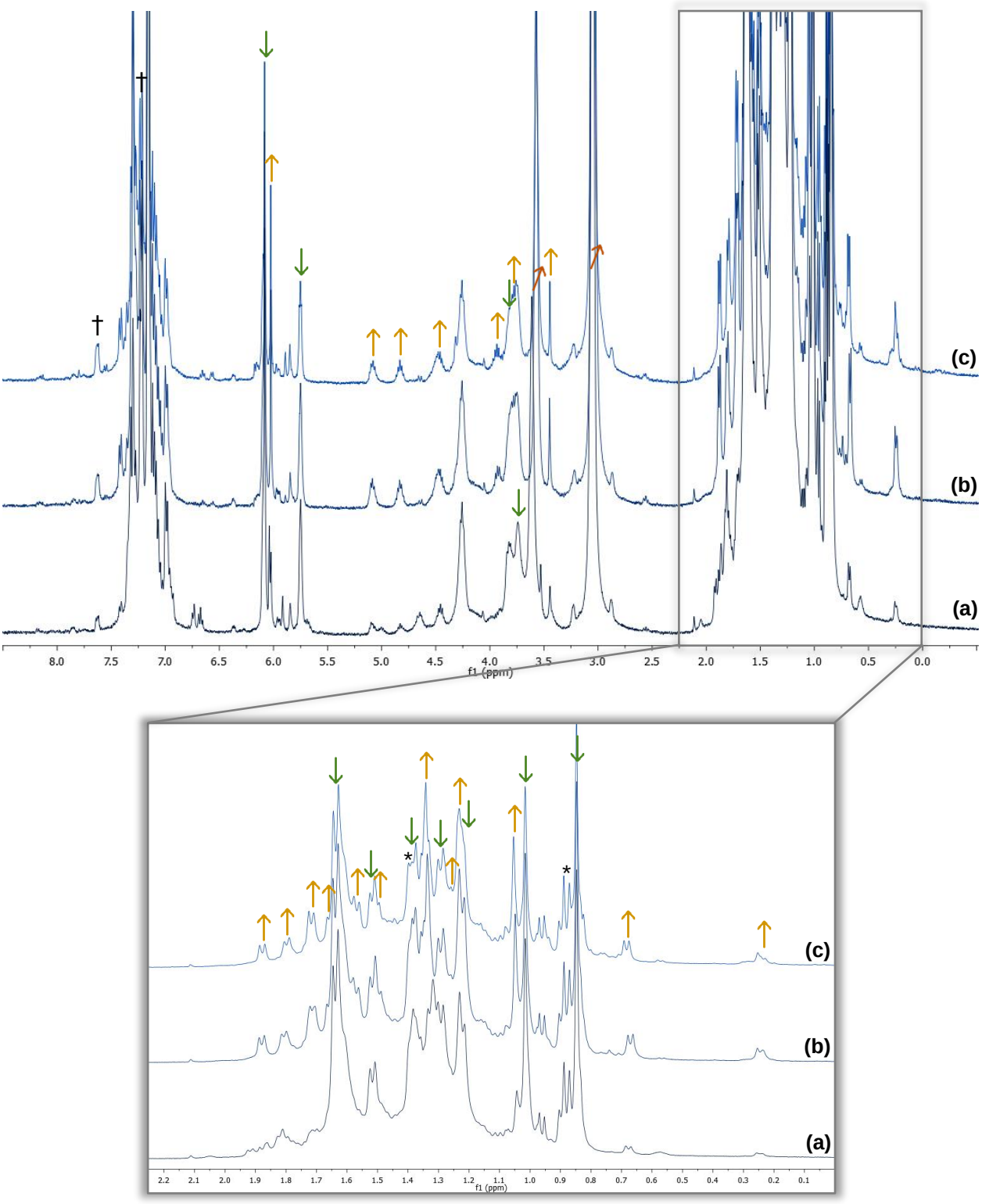

Figure S15. ^{1}H NMR spectral array following the room temperature decomposition of **Sc^{naph}** to form **Sc$^{C\text{-}H}$·THF** and naphthalene (25 ˚C, 400 MHz, C_6D_6). (a) 0 d, (b) 1.5 d, (c) 4d. Resonances marked with ↓ denote **Sc^{naph}** and resonances marked with ↑ denote formation of **Sc$^{C\text{-}H}$·Et$_2$O** (**Sc$^{C\text{-}H}$-taut**). ∗, † denote the presence of residual hexanes and naphthalene.

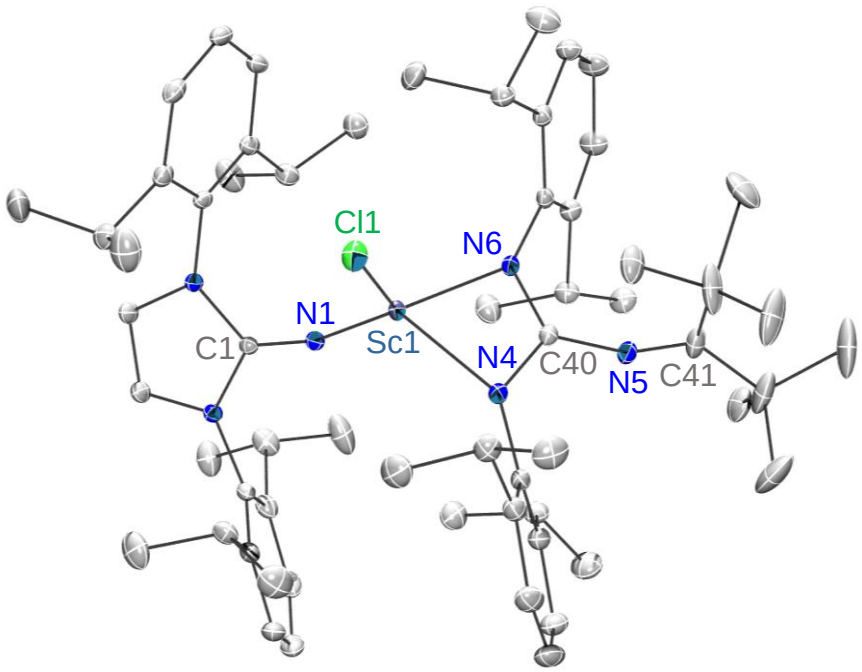

Figure S16. Solid-state molecular structure of $\mathbf{Sc^{Cl}}\cdot 0.5C_7H_8$ with 30% probability ellipsoids. Hydrogen atoms and co-crystallized toluene molecule are omitted for clarity. Selected bond lengths (Å) and angles (deg): Sc1-N1 = 1.932(1), N1-C1 = 1.279(2), N4-C40 = 1.348(2), N5-C40 = 1.368(2), N6-C40 = 1.347(2), N5-C41 = 1.274(2), Sc1-N1-C1 = 160.3(1), C40-N5-C41 = 139.0(2).

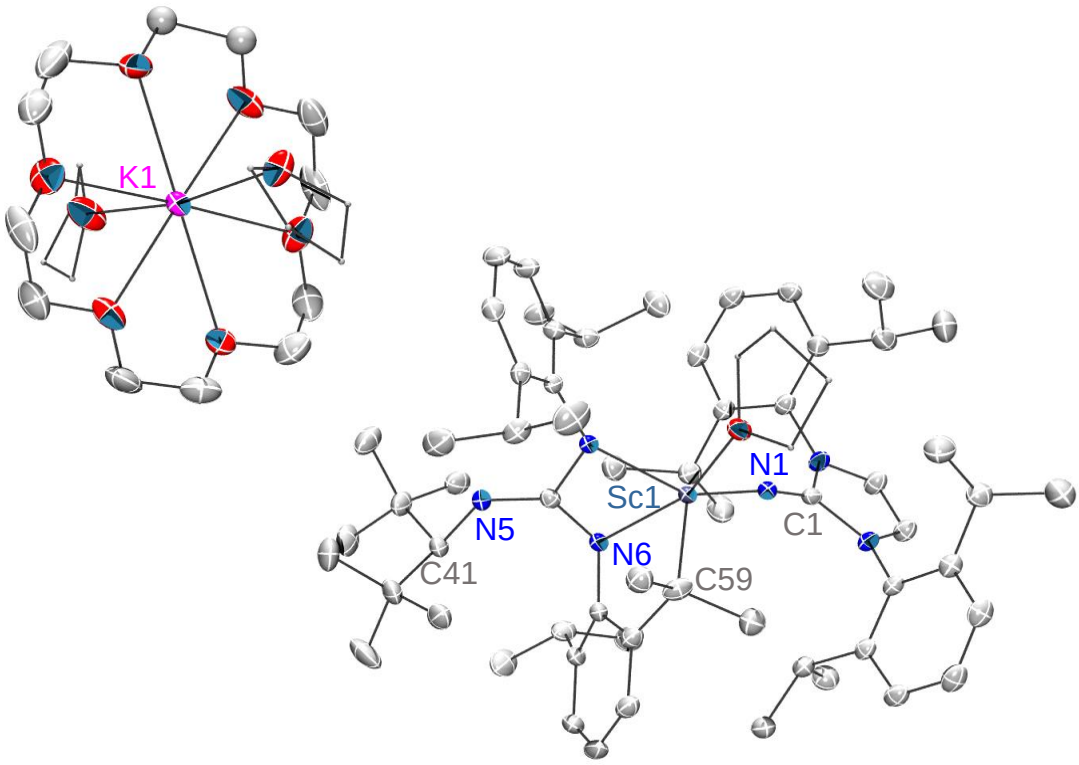

Figure S17. Solid-state molecular structure of **Sc$^{C\text{-}H}$·THF** with 30% probability ellipsoids. Hydrogen atoms and co-crystallized solvent molecules are omitted for clarity.

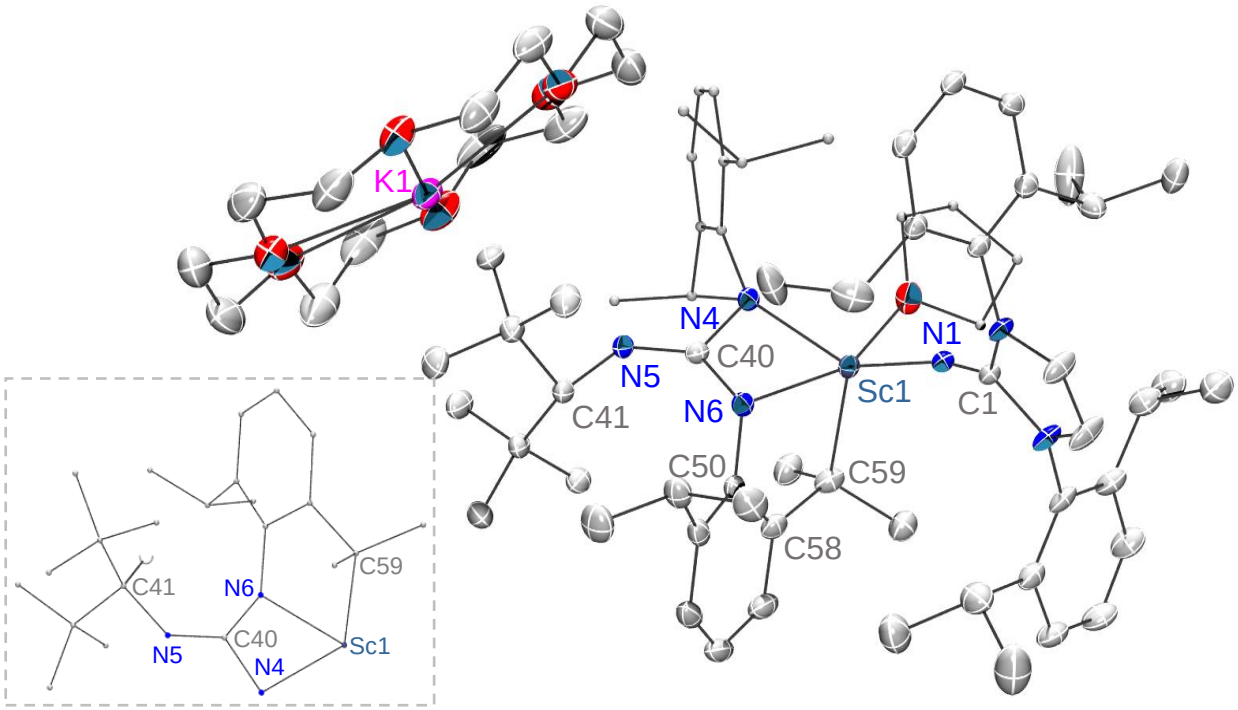

Figure S18. Solid-state molecular structure of **$Sc^{C\text{-}H}$·Et_2O** with 30% probability ellipsoids. Crown-coordinated and co-crystallized Et_2O molecules and hydrogen atoms are omitted for clarity. Selected bond lengths (Å) and angles (deg) in molecule 1: Sc1-N1 = 2.043(2), Sc1-C59 = 2.315(3), N1-C1 = 1.249(4), N4-C40 = 1.390(4), N5-C40 = 1.295(4), N5-C41 = 1.453(4), N6-C40 = 1.413(4), Sc1-N1-C1 = 162.4(2), Sc1-C59-C58 = 102.8(2), C40-N5-C41 = 122.6(3). Selected bond lengths (Å) and angles (deg) in molecule 2 (not shown): Sc2-N7 = 2.037(3), Sc2-C136 = 2.298(3), N7-C78 = 1.246(4), N10-C117 = 1.390(4), N11-C117 = 1.299(4), N11-C118 = 1.452(4), N12-C117 = 1.412(4), Sc2-N7-C78 = 173.8(2), Sc2-C136-C135 = 101.0(2), C117-N11-C118 = 123.1(3).

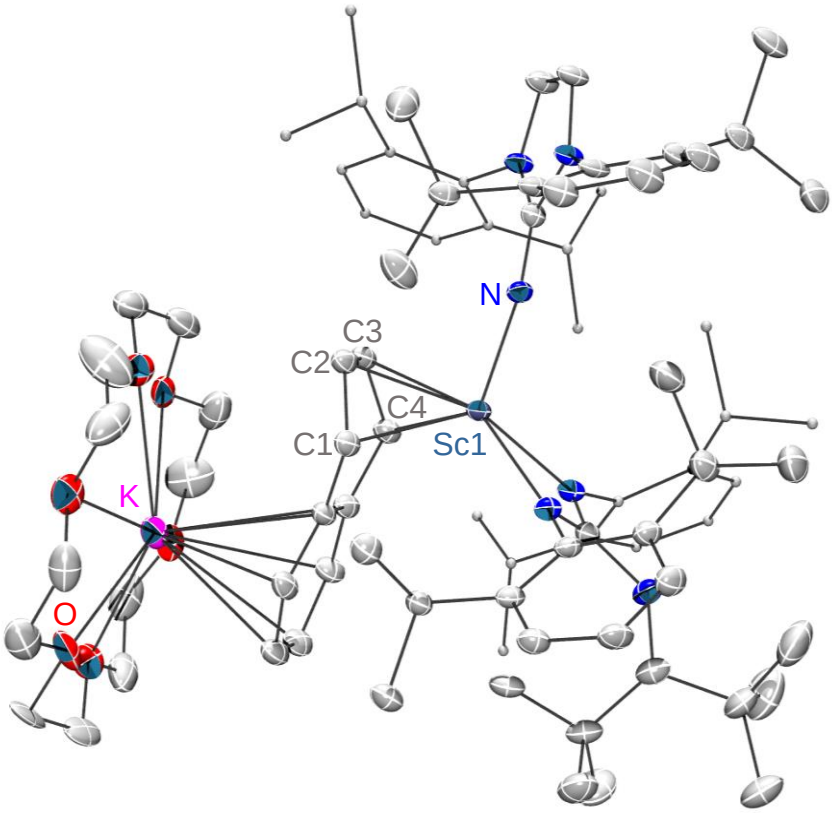

Figure S19. Solid-state molecular structure of **Sc^{naph}** with 30% probability ellipsoids. Hydrogen atoms are omitted for clarity. Structure presented for connectivity only.

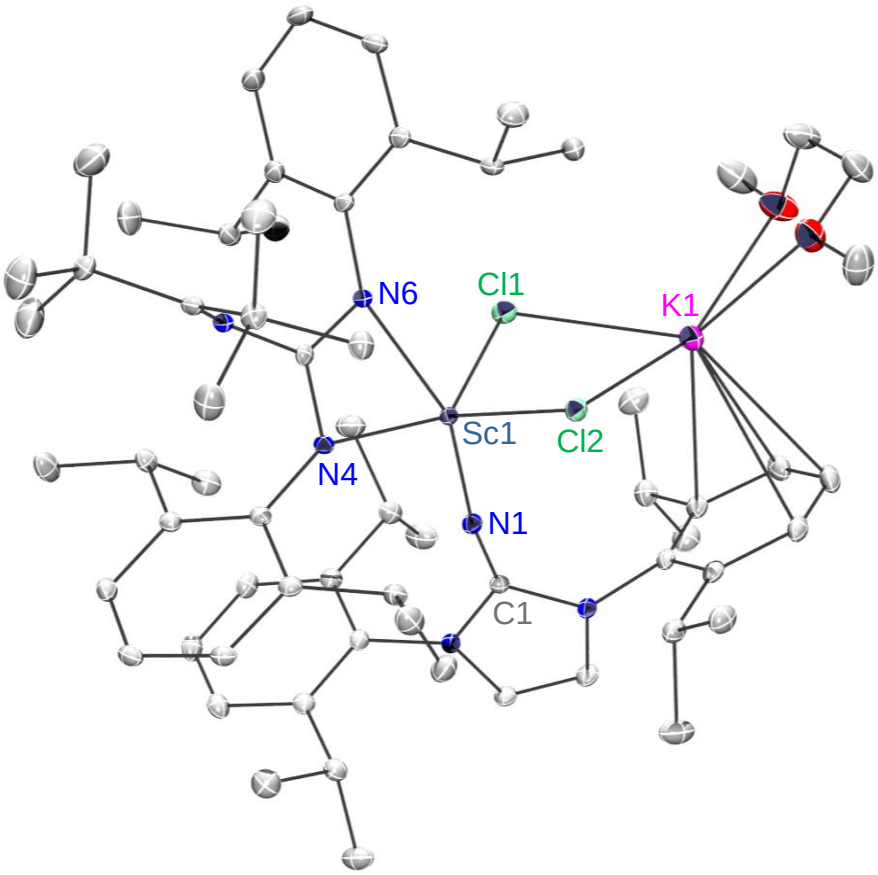

Figure S20. Solid-state molecular structure of [(^{ket}guan)(^{Dipp}ImN)Sc(μ-Cl)$_2$K(DME)]·C_6H_{14} with 30% probability ellipsoids. Hydrogen atoms and non-coordinated hexanes molecule are omitted for clarity. Selected bond lengths (Å) and angles (deg): Sc1-Cl1 = 2.4843(5), Sc1-Cl2 = 2.4427(5), Sc1-N1 = 1.968(1), Sc1-N4 = 2.202(1), Sc1-N6 = 2.257(1), N1-C1 = 1.261(2), K1-Cl1 = 2.9932(6), K1-Cl2 = 3.052(5), Sc1-N1-C1 = 170.0(1).

Table S1. X-ray crystallographic data for complexes $\mathbf{Sc^{Cl}}$, $\mathbf{Sc^{C\text{-}H}\cdot Et_2O}$, $\mathbf{Sc^{C\text{-}H}\cdot THF}$, $\mathbf{Sc^{Naph}}$, and $[(^{ket}guan)(^{Dipp}ImN)Sc(\mu\text{-}Cl)_2K(DME)]\cdot C_6H_{14}$

	$Sc^{Cl}\cdot 0.5C_7H_8$	$Sc^{C\text{-}H}\cdot Et_2O$	$Sc^{C\text{-}H}\cdot THF$
Empirical formula	$C_{61}ClH_{88}N_6Sc\cdot 0.5C_7H_8$	$C_{81}H_{120}KN_6O_8Sc\cdot 0.5C_4H_{10}O$	$C_{85}H_{135}KN_6O_9Sc$
Formula weight (g/mol)	1039.05	1427.19	1469.04
Crystal habit, color	thick needle, colorless	plate, colorless	plate, colorless
Crystal size (mm)	0.21 × 0.06 × 0.04	0.15 × 0.13 × 0.05	0.12 × 0.08 × 0.04
Crystal system	Monoclinic	Monoclinic	Triclinic
Space group	$P2_1/c$	$P2_1/c$	$P\bar{1}$
Volume (Å^3)	6041.1(3)	16683.7(15)	4928.0(4)
a (Å)	25.6178(8)	18.7947(10)	12.7099(6)
b (Å)	12.2477(3)	22.7491(12)	17.8534(9)
c (Å)	19.3231(5)	39.275(2)	23.1786(13)
α°	90	90	105.198(2)
β°	94.8450(10)	96.525(2)	100.704(2)
γ°	90	90	95.573(2)
Z	4	12	2
Absorption coefficient (mm^{-1})	0.209	0.194	0.166
F_{000}	2220.0	6240.0	1598.0
Total number of reflections collected	160463	529246	219773
Unique reflections	13320	31738	18635
R_1 and wR_2 indices [$I \geq 2\sigma(I)$]	0.0406; 0.1040	0.0730; 0.1792	0.0756; 0.2151
R_1 and wR_2 indices [all data]	0.0477; 0.1097	0.1020; 0.2006	0.0859; 0.2255
Largest diff. peak and hole (eÅ^{-3})	0.56/-0.31	0.69/-0.72	1.05/-0.93
GoF	1.021	1.040	1.062

	Sc^{Naph}	$[(^{ket}guan)(^{Dipp}ImN)Sc(\mu\text{-}Cl)_2K(DME)]\cdot C_6H_{14}$
Empirical formula	$C_{83}H_{120}KN_6O_6Sc$	$C_{65}Cl_2H_{98}KN_6O_2Sc\cdot C_6H_{14}$
Formula weight (g/mol)	1381.93	1236.64
Crystal habit, color	rhombohedral, dark red	Block, colorless
Crystal size (mm)	0.11 × 0.09 × 0.07	0.06 × 0.09 × 0.10
Crystal system	Monoclinic	Monoclinic
Space group	$P2_1/c$	$P2_1/n$
Volume (Å^3)	10926.3(1)	7297.0(4)
a (Å)	22.1007(14)	22.5754(7)
b (Å)	20.4848(11)	13.3421(4)
c (Å)	26.1601(16)	25.6446(8)
α°	90	90
β°	112.696(2)	109.1460(10)
γ°	90	90
Z	6	6
Absorption coefficient (mm^{-1})	0.145	0.276
F_{000}	2991.0	2680.0
Total number of reflections collected	183081	198110
Unique reflections	13766	13851
R_1 and wR_2 indices [I ≥2σ(I)]	0.0723; 0.2359	0.0349; 0.0844
R_1 and wR_2 indices [all data]	0.0910; 0.2481	0.0445; 0.0902
Largest diff. peak and hole (eÅ^{-3})	0.30/-0.28	0.92/-0.42
GoF	1.166	1.023

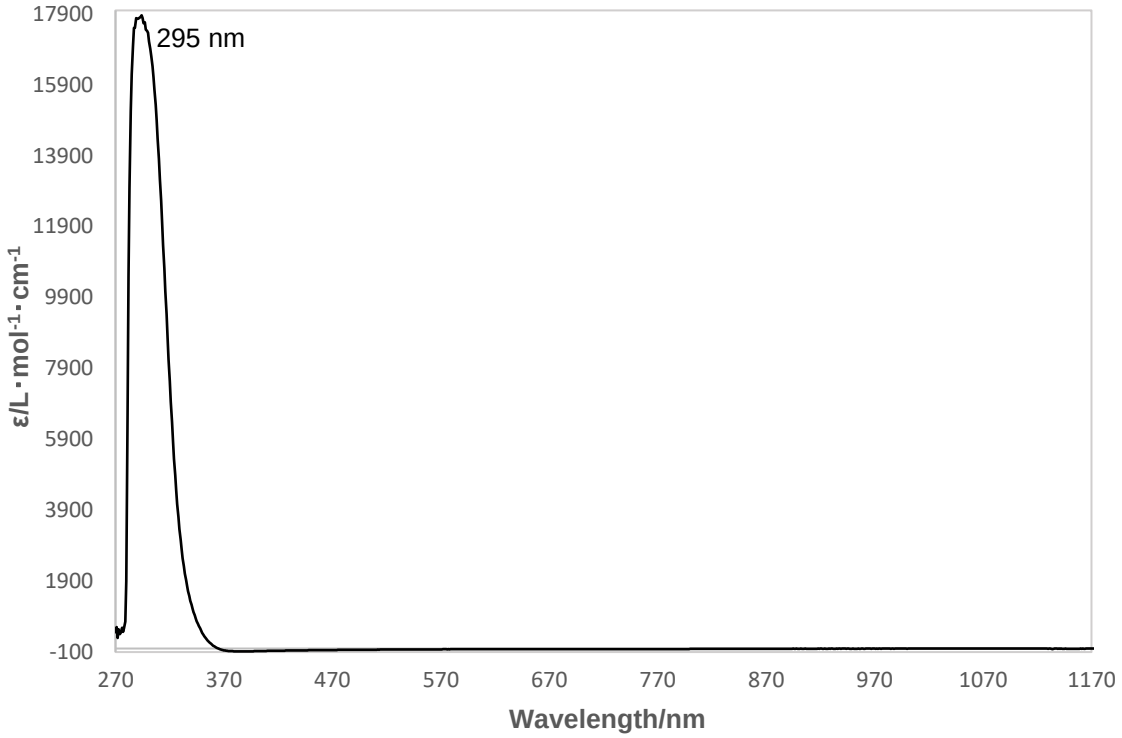

Figure S21. Room temperature electronic absorption spectrum of **Sc^{Cl}**·0.5C_7H_8 (C_7H_8, 0.207 mM).

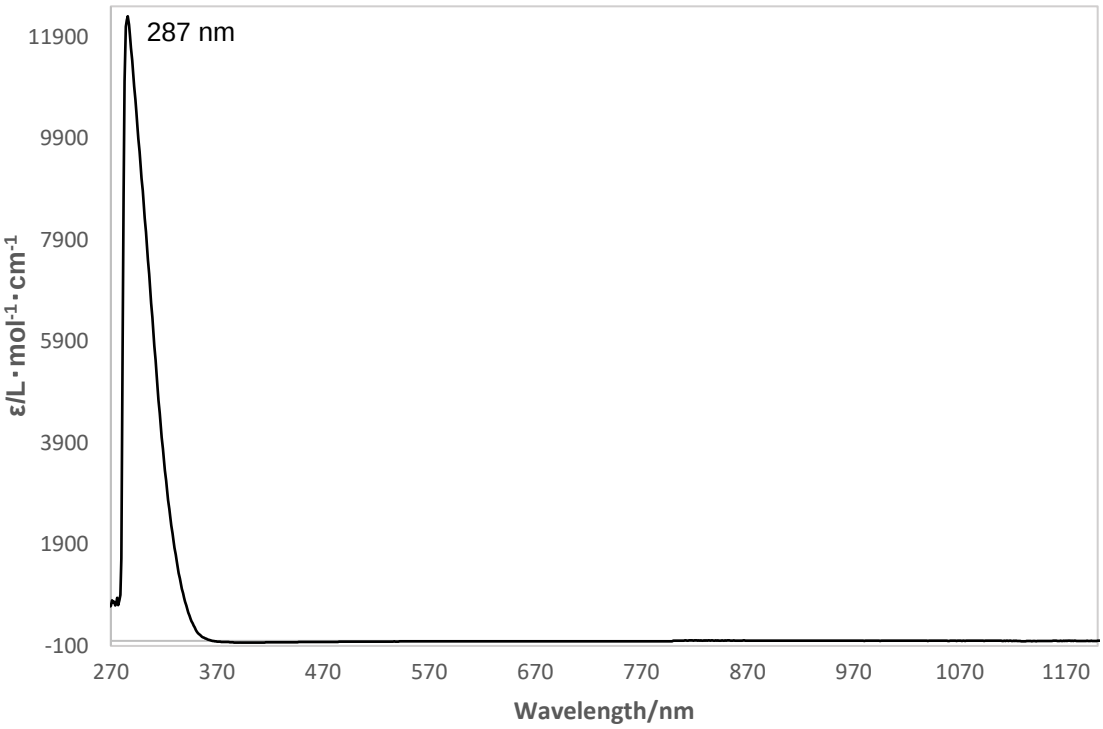

Figure S22. Room temperature electronic absorption spectrum of **$Sc^{C\text{-}H}$·Et_2O** (**$Sc^{C\text{-}H}$-taut**) (C_7H_8, 0.234 mM).

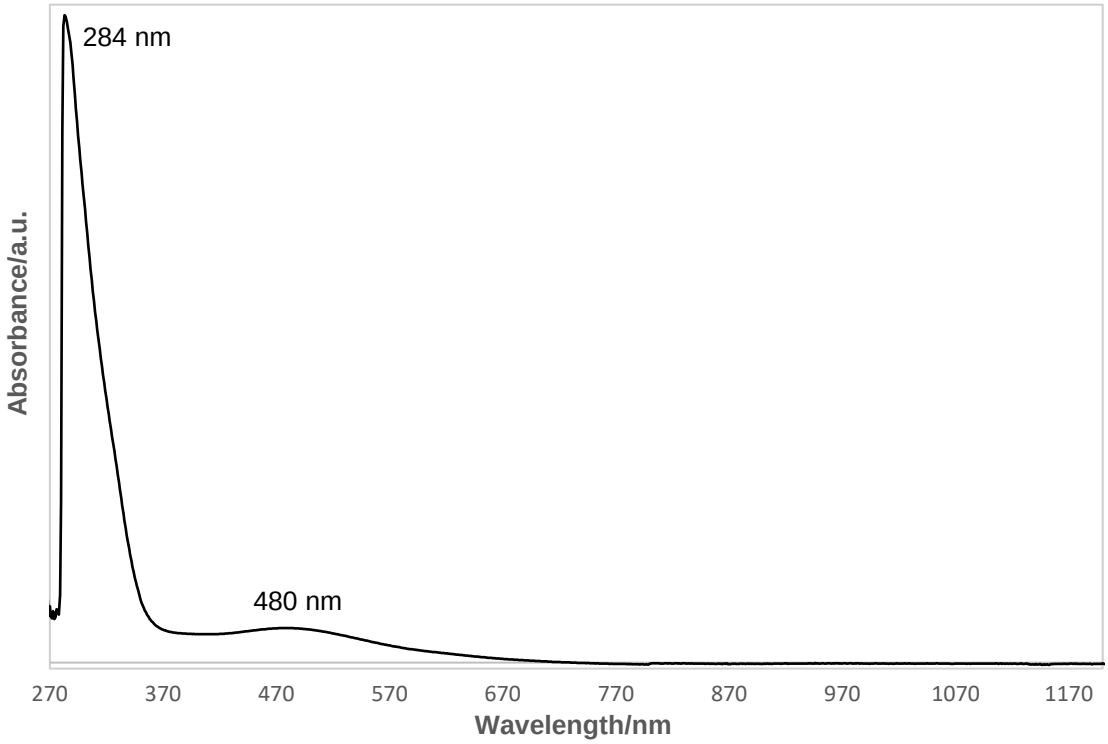

Figure S23. Room temperature electronic absorption spectrum of **Sc^{naph}** (C_7H_8) with absorption presented in arbitrary units.

References

1. Panda, T. K.; Trambitas, A. G.; Bannenberg, T.; Hrib, C. G.; Randoll, S.; Jones, P. G.; Tamm, M., Imidazolin-2-iminato Complexes of Rare Earth Metals with Very Short Metal−Nitrogen Bonds: Experimental and Theoretical Studies. *Inorg. Chem.* **2009**, *48*, 5462-5472.
2. Maity, A. K.; Metta-Magaña, A. J.; Fortier, S., Donor Properties of a New Class of Guanidinate Ligands Possessing Ketimine Backbones: A Comparative Study Using Iron. *Inorg. Chem.* **2015**, *54*, 10030-10041.
3. Gokel, G. W.; Cram, D. J.; Liotta, C. L.; Harris, H. P.; Cook, F. L., Preparation and purification of 18-crown-6[1,4,7,10,13,16-hexaoxacyclooctadecane]. *J. Org. Chem.* **1974**, *39*, 2445-2446.
4. SMART APEX II. *Bruker AXS Inc. Madison, WI*.
5. SAINT Software User's Guide. *Bruker AXS Inc. Madison, WI*.
6. Blessing, R., An empirical correction for absorption anisotropy. *Acta Crystallographica Section A* **1995**, *51*, 33-38.
7. Sheldrick, G. M., SHELXTL. *Bruker AXS Inc. Madison, WI*.
8. Dolomanov, O. V.; Bourhis, L. J.; Gildea, R. J.; Howard, J. A. K.; Puschmann, H., OLEX2: a complete structure solution, refinement and analysis program. *J. Appl. Crystallogr.* **2009**, *42*, 339-341.
9. Spek, A., PLATON SQUEEZE: a tool for the calculation of the disordered solvent contribution to the calculated structure factors. *Acta Crystallogr. C* **2015**, *71*, 9-18.